An Alternative Multiresolution Basis in EFIE for Analysis of Low-Frequency Problems

Jianjun Ding, Jian Zhu, Ru-shan Chen, Z. H. Fan, and K. W. Leung

Department of Electronic Engineering
Nanjing University of Science and Technology, Nanjing, 210094, China
draksea@yahoo.com, zhujian82gogo@hotmail.com, eerschen@mail.njust.edu.cn,
zhfan@mail.njust.edu.cn, eekleung@cityu.edu.hk

Abstract ― An alternative multiresolution (MR) basis is presented for the method-of-moments (MoM) solution of the electric-field integral equation (EFIE) for the analysis of low-frequency problems. The proposed MR basis functions can be treated as an extension of the traditional loop-tree basis function to hierarchical functions. Similar to the loop-tree basis, the MR basis functions are linear combinations of standard Rao-Wilton-Glisson (RWG) functions. Therefore, the MR algorithm can be easily applied to MoM codes with RWG basis. Since the MR basis is immune from the so-called low-frequency breakdown, the MR basis is especially suitable for the analysis of low-frequency problems. Compared with the previous MR basis, the present MR basis is easier to construct and comprehend, and the basis-changing matrix is sparser. Physical interpretation and comparison are given for the previous and present MR bases. Numerical results demonstrate that both the previous and present MR bases are efficient for 3D electromagnetic scattering problems at low frequencies.

Index Terms ― EFIE, electromagnetic scattering, low frequency, method of moments (MoM), multiresolution techniques.

I. INTRODUCTION

The method of moments (MoM) is one of the most powerful numerical methods applicable to a wide variety of practical electromagnetic radiation and scattering problems [1, 2]. The electric field integral equation (EFIE) is always preferred in MoM. However, the EFIE suffers the so called low-frequency breakdown problem which occurs when the harmonic field wavelength is substantially larger than the characteristic size of the MoM grid. An effective solution to this problem is to separate the solenoidal part of the current [3-11]. The loop-star basis and loop-tree basis are proposed in the early 1980s [3, 4]. Both of them introduce divergence-free loop functions which can effectively separate the solenoidal part of the current. The detailed discussion and application of the loop-star basis and loop-tree basis can be found in [5-9], and a comparison of the frequency dependent iterative solver convergence for RWG, loop-tree, and loop-star basis functions is given in [10].

In recent years, the multiresolution (MR) basis has been proposed and acted as an efficient physics-based preconditioner [12-27]. Compared with the loop-star/tree basis, the MR basis has a much faster MoM convergence rate when an iterative solver is applied. The reasons why the MR basis can positively act on the spectrum of a MoM matrix has been investigated and discussed in [20, 21]. The MR basis was first mentioned by G. Vecchi in [7], where he pointed out that a MR basis can be efficiently constructed to replace the loop-star basis. Consequently, a MR basis was proposed in [12]. Then a modified MR basis was proposed in [13] to simplify the generation procedure. However, the MR bases in [12, 13] has a limit in modeling the curved structures, since the shape of the hierarchical meshes is restricted by the coarse mesh. To remedy this drawback of MR basis, a curvilinear MR basis is proposed in [15]. More recently, a new MR algorithm was proposed in [16-19] to overcome the shortcoming of the MR basis defined over triangular patches. In the new MR algorithm, the concepts of generalized mesh and generalized RWG (gRWG) basis were introduced. The generalized mesh is generated by

a grouping algorithm. The gRWG basis is the generalization of the standard RWG basis and it is defined on the generalized meshes. The new MR basis functions are constructed as linear combinations of gRWG basis functions and can finally be represented by linear combinations of the RWG basis functions.

Inspired by the novel idea of generalized mesh and generalized RWG basis, an alternative MR basis is proposed in this paper which is also defined on the generalized meshes. Contrary to the MR algorithm in [16-19] which relies on mathematical operations, the MR basis proposed in this paper is generated via geometric operations. Compared with the previous MR basis, the proposed MR basis can be constructed in a much easier fashion and provide more direct physical meanings. Also, the basis-changing matrix of the RWG basis functions to the MR basis functions is sparser and can be generated faster. Furthermore, physical interpretations are provided for both MR bases and the number of MR basis functions of each level is clearly given which explains why the MR bases span the same space as the RWG basis. Numerical examples demonstrate that the MR bases have a much faster convergence rate for iterative solvers than the traditional loop-tree basis as explained in [20, 21].

This paper is organized as follows. Section II introduces the hierarchical generalized meshes and the gRWG basis. Section III gives a detailed description of the MR basis generation. Section IV provides physical interpretations for the MR bases. A discussion on the computational complexity of the MR basis is given in Section V. Section VI presents numerical results to validate and demonstrate the performance of the MR basis. Finally, the work is concluded in Section VII.

II. GENERALIZED MESH AND GRWG BASIS

Before discussing the new MR basis, the essential concepts of the generalized mesh and gRWG basis are briefly described as preliminary knowledge. Since the detailed generation algorithm of the generalized mesh and gRWG basis has already been given in [17, 18], only a brief description is provided in this section.

A. Hierarchical generalized meshes

Generation of the hierarchical generalized meshes starts from an input triangular mesh which is called level-0 mesh and denoted by M^0. Using a grouping algorithm, the nearby cells of the level-0 mesh are grouped into level-1cells. The union of the level-1 cells is called level-1 mesh, M^1. Applying the same grouping algorithm to the level-1 cells will generate the level-2 mesh (M^2) and so on and a set of hierarchical generalized meshes $\{M^l,\ l = 1, \ldots, L\}$ will be obtained. The last level L is usually decided by the maximum size of the generated cells that should be smaller than the wavelength, with a typical range of $\lambda/8 - \lambda/4$. To demonstrate the grouping algorithm, the hierarchical generalized meshes of a circular plate are shown in Fig. 1.

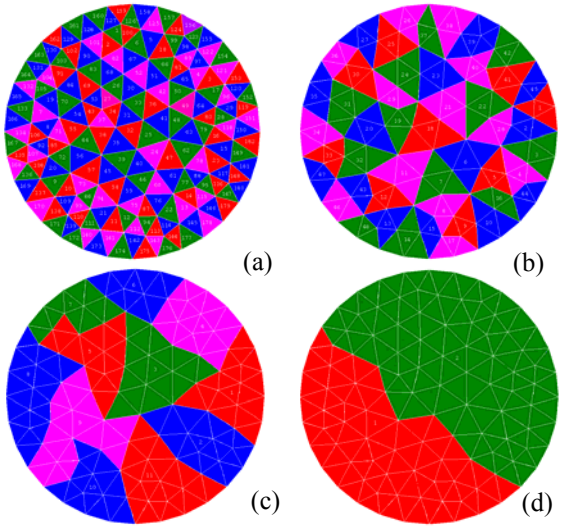

Fig. 1. An example of hierarchical generalized meshes on a circular plate. (a) level-0 mesh, (b) level-1 mesh, (c) level-2 mesh, (d) level-3 mesh.

B. Generalized RWG basis

Similar to the definition of the RWG basis, a gRWG basis function is defined on a pair of adjacent cells of its corresponding level. Denoting a level-l gRWG basis function as $\bar{R}_i^l(\bar{r})$, its divergence is given as

$$\nabla_s \cdot \bar{R}_i^l(\bar{r}) = \begin{cases} \ell_i^l / A_{+,i}^l & \bar{r} \in C_{+,i}^l \\ -\ell_i^l / A_{-,i}^l & \bar{r} \in C_{-,i}^l \\ 0 & \text{otherwise,} \end{cases} \tag{1}$$

where $A_{+,i}^l$ and $A_{-,i}^l$ are the areas of the two adjacent cells ($C_{+,i}^l$, $C_{-,i}^l$), and ℓ_i^l is the length of the level-*l* generalize edge shared by the two cells and is a polygonal line in general.

C. Inter-mesh reconstruction relationship

The inter-mesh reconstruction relationship can be derived through the charge matrix. In the inter-mesh reconstruction relationship, a level-*l* *g*RWG function $\vec{R}_i^l(\vec{r})$ can be expressed as the linear combination of the level-(*l*-1) gRWG functions $\vec{R}_n^{l-1}(\vec{r})$ (n = 1,…, N_i^{l-1}) which are completely defined in the domain $C_{+,i}^l \cup C_{-,i}^l$ of $\vec{R}_i^l(\vec{r})$, i.e.

$$\vec{R}_i^l(\vec{r}) = \sum_{n=1}^{N_i^{l-1}} R_{n,i}^l \vec{R}_n^{l-1}(\vec{r}), \tag{2}$$

where $R_{n,i}^l$ is the reconstruction coefficient. Applying the surface divergence to both sides of (2), we have

$$\nabla_s \cdot \vec{R}_i^l(\vec{r}) = \sum_{n=1}^{N_i^{l-1}} R_{n,i}^l \nabla_s \cdot \vec{R}_n^{l-1}(\vec{r}). \tag{3}$$

Projecting (3) on the cells C_m^{l-1} (m = 1, …, $N_{c,i}^{l-1}$) in the domain of $\vec{R}_i^l(\vec{r})$, a linear system can be obtained as

$$\left[Q_i^l\right] \cdot \left[R_i^l\right] = \left[q_i^l\right], \tag{4}$$

where $\left[Q_i^l\right]$ is the $N_{c,i}^{l-1} \times N_i^{l-1}$ charge matrix whose element is given by

$$\left[Q_i^l\right]_{m,n} = \nabla_s \cdot \vec{R}_n^{l-1}(\vec{r})\Big|_{C_m^{l-1}},$$

$$\left[R_i^l\right] = \left[R_{1,i}^l, R_{2,i}^l, \ldots, R_{N_i^{l-1},i}^l\right]^T, \left[q_i^l\right]_m = \nabla_s \cdot \vec{R}_n^l(\vec{r})\Big|_{C_m^{l-1}}.$$

As will be discussed in the next section, the maximum number of the linear independent functions $\vec{R}_n^{l-1}(\vec{r})$ (n = 1,…, N_i^{l-1}) is $N_{c,i}^{l-1} - 1$ according to Euler's theorem. Therefore, the rank of the matrix $\left[Q_i^l\right]$ is $N_{c,i}^{l-1} - 1$ and a full row rank matrix $\left[\tilde{Q}_i^l\right]$ can be obtained by deleting an arbitrary row of $\left[Q_i^l\right]$. When $N_{c,i}^{l-1} - 1 < N_i^{l-1}$, the matrix equation (4) has infinitely many solutions and the least squares solution can be taken as the reconstruction coefficients $\left[R_i^l\right]$, i.e.

$$\left[R_i^l\right] = \left[\tilde{Q}_i^l\right]^+ \left[q_i^l\right], \tag{5}$$

where $\left[\tilde{Q}_i^l\right]^+$ is the Moore-Penrose pseudoinverse of $\left[\tilde{Q}_i^l\right]$.

III. MR BASIS GENERATION

For a general 3-D surface (without torus), the Euler's theorem states that [9, 19]

$$V + F = E - N_\Gamma + 2, \tag{6}$$

where V, E, F, N_Γ denote the number of vertices, edges, faces, and separated boundary contours, respectively. Since the number of vertices and edges on the boundary contours is equal, we have

$$V_{\text{int}} + F = E_{\text{int}} - N_\Gamma + 2, \tag{7}$$

where V_{int}, E_{int} is the number of internal vertices and edges, respectively.

For a domain (e.g. a cell or a pair of cells of level-*l*) composed of $N_{c,i}^{l-1}$ cells of level-(*l*-1), we have

$$N_i^{l-1} - (V_{\text{int}} + N_\Gamma - 1) = N_{c,i}^{l-1} - 1. \tag{8}$$

N_i^{l-1} is the number of the gRWG functions in the domain, since the gRWG functions are defined on the interior edges. If connecting all the cells in a tree (see e.g. Fig. 2) and avoid forming any loop on the tree, then the maximum number of edges on the tree will be $N_{c,i}^{l-1} - 1$. Obviously, the gRWG functions corresponding to the edges on the tree are linear independent. Therefore, the maximum number of the linear independent gRWG functions in the domain is equal to $N_{c,i}^{l-1} - 1$.

If the surface is discretized with triangles, the number of solenoidal functions N_S and the number of nonsolenoidal functions N_X of loop-star basis are given by [7, 9]

$$N_S = V_{\text{int}} + N_\Gamma - 1 \tag{9}$$

$$N_X = F - 1. \tag{10}$$

Their sum is equal to the number of the RWG functions, i.e.

$$N_S + N_X = N, \tag{11}$$

where N is the number of the RWG functions.

Similar to loop-star/tree basis, the MR basis can also be split into the solenoidal and nonsolenoidal parts. It will be shown in the next section that the solenoidal and nonsolenoidal functions of the MR basis span the same space as for the loop-tree/star basis, and the numbers of the solenoidal and nonsolenoidal functions of the MR basis can also be given by equations (9)-(11).

A. Solenoidal basis

It has already been shown in [17] that the use of a hierarchical decomposition of the nonsolenoidal part together with a non hierarchical loop basis suffices to obtain well conditioned MoM matrices and, hence, quickly convergent solvers for low-frequency and very dense discretizations. The difference between the low-frequency and very dense discretization is addressed in [11]. Therefore, for simplicity, the loop basis generated on level-0 mesh is chosen as the solenoidal part of the MR basis. The detailed discussion of the loop basis can be found in [7, 9], whereas the topic of generating the loop basis functions on the more complex surfaces (e.g. wire-surface structure) can be found in [28].

After generating the loop basis, the solenoidal basis of the MR basis can be written as

$$\left[\vec{f}_L\right]=\left[T_L\right]^T\left[\vec{R}^0\right], \tag{12}$$

where $\left[\vec{f}_L\right]^T=\left[\vec{f}_{1,L},\vec{f}_{2,L},\ldots,\vec{f}_{N_S,L}\right]$ is the solenoidal MR basis, $\left[T_L\right]$ is the basis-changing matrix, and $\left[\vec{R}^0\right]^T=\left[\vec{R}_1^0,\vec{R}_2^0,\ldots,\vec{R}_N^0\right]$ is the RWG basis of level-0 mesh.

B. Nonsolenoidal basis

The nonsolenoidal basis is defined on the hierarchical generalized meshes. The nonsolenoidal basis functions of the highest level (level-*L*) are different from the nonsolenoidal basis functions of other levels (level-*l*, l = 1, …, *L*-1). Therefore, the nonsolenoidal basis functions of level-*L* are generated separately from the function of the other levels.

1). Nonsolenoidal functions of level-L

The generation of the nonsolenoidal functions of level-*L* is similar to that of the tree basis functions in loop-tree basis. The only difference is that the cells of level-*L* are replaced by triangles. An easy procedure of constructing the nonsolenoidal functions of level-*L* is to connect the cells of the level-*L* mesh in a tree, and each gRWG basis function on the branch of the tree is taken as a nonsolenoidal function. To demonstrate this procedure, the nonsolenoidal functions defined on the level-2 mesh (Fig. 1) are plotted. In this example, it is assumed that level-2 mesh is of the highest level. As shown in Fig. 2 (a), each black line connecting a pair of cells represents a generated nonsolenoidal function. It is worth mentioning that the number of the nonsolenoidal functions of level-*L* equals the number of the cells of level-*L* minus one.

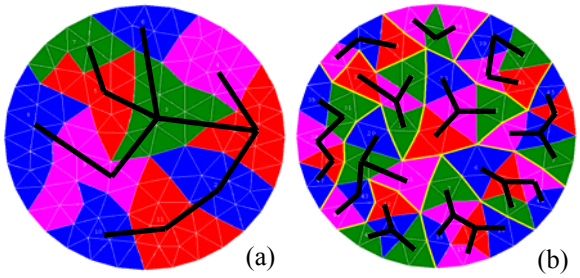

Fig. 2. The nonsolenoidal functions, which are depicted with black lines, on a circular plate. (a) Level-2 functions, (b) level-1 functions.

2). Nonsolenoidal functions of level- l (l = 1, …, L-1)

Let the nonsolenoidal functions of level-*l* belong to the cell C_k^{l+1} of level-(*l*+1) denoted with $\left\{\vec{f}_{k,i}^{\,l}, i=1,\cdots,N_{C_k^{l+1}}^l-1\right\}$, in which $N_{C_k^{l+1}}^l$ is the number of the cells of level-*l* belonging to the cell C_k^{l+1}, the nonsolenoidal functions of level-*l* can be expressed as the union of the nonsolenoidal functions that belong to all the cells of level-(*l*+1), i.e.

$$\left\{\vec{f}_{j,X}^{\,l}, j=1,\cdots,N_c^l-N_c^{l+1}\right\}=\bigcup_{k=1}^{N_c^{l+1}}\left\{\vec{f}_{k,i}^{\,l}, i=1,\cdots,N_{C_k^{l+1}}^l-1\right\}, \tag{13}$$

where N_c^l and N_c^{l+1} are the numbers of the cells of level-*l* and level-(*l*+1) respectively, and $N_c^l-N_c^{l+1}$ is the number of the nonsolenoidal functions of level-*l*. A simple way of generating the level-*l* nonsolenoidal functions in the cell C_k^{l+1} is to connect all the level-*l* cells which are completely included in the cell C_k^{l+1} in a tree and taking the gRWG basis functions on the branches of the tree as nonsolenoidal functions. An example of level-1 nonsolenoidal functions is shown in Fig. 2 (b). As can be observed from Fig. 2 (b), the level-2 cells are bounded with yellow lines and the level-1 nonsolenoidal functions are clustered in each level-2 cell shown with black lines.

The nonsolenoidal functions (13) can be written as linear combinations of the gRWG basis functions of level-*l*, i.e.

$$\left[\vec{f}_X^{\,l}\right] = \left[T'^{\,l}_{\ X}\right]^T \left[\vec{R}^l\right], \tag{14}$$

where $\left[\vec{f}_X^{\,l}\right]^T = \left[\vec{f}^{\,l}_{1,X}, \vec{f}^{\,l}_{2,X}, \ldots, \vec{f}^{\,l}_{N_c^l - N_c^{l+1},X}\right]$, $\left[T'^{\,l}_{\ X}\right]^T$ is the basis-changing matrix, and $\left[\vec{R}^l\right]^T = \left[\vec{R}^l_1, \vec{R}^l_2, \ldots, \vec{R}^l_{N^l}\right]$ is the gRWG basis of level-*l*. Applying the inter-mesh reconstruction relationship (2) recurrently, the nonsolenoidal functions of level-*l* can then be written as linear combinations of the RWG basis functions of level-0 mesh, i.e.,

$$\left[\vec{f}_X^{\,l}\right] = \left[T_X^l\right]^T \left[\vec{R}^0\right]. \tag{15}$$

Then, the nonsolenoidal functions of all levels can be written as

$$\left[\vec{f}_X\right] = \left[T_X\right]^T \left[\vec{R}^0\right], \tag{16}$$

where $\left[\vec{f}_X\right]^T = \left[\left[\vec{f}_X^{\,0}\right]^T, \left[\vec{f}_X^{\,1}\right]^T, \cdots, \left[\vec{f}_X^{\,L}\right]^T\right]$ and $\left[T_X\right]^T = \left[\left[T_X^0\right]^T, \left[T_X^1\right]^T, \cdots, \left[T_X^L\right]^T\right]$.

Finally, the MR basis functions can be expressed in terms of the RWG basis functions as follows

$$\left[\vec{f}_{MR}\right] = \left[T\right]^T \left[\vec{R}^0\right], \tag{17}$$

where $\left[T\right] = \left[\left[T_L\right], \left[T_X\right]\right]$.

IV. PHYSICAL INTERPRETATION OF MR BASES

Although the generation algorithm of the MR basis proposed in [18, 19] is clearly given, the physical meaning behind it is not clearly pointed out. Readers may also be confused about why the number of the MR basis functions equals the number of the RWG basis functions. Therefore, physic interpretations are tried to give in this section for both the present MR basis and the previous MR basis for better understanding of the MR bases.

A. The present MR basis

From the discussion given in Section III-B, the total number of the nonsolenoidal functions can be calculated as

$$\begin{aligned} N_X &= N_X^0 + N_X^1 + \cdots + N_X^L \\ &= (F - N_c^1) + (N_c^1 - N_c^2) + \cdots + (N_c^L - 1) \cdot \\ &= F - 1 \end{aligned} \tag{18}$$

Therefore, the numbers of the nonsolenoidal functions of the MR basis also satisfy (10). Similar to the loop-tree/star basis, it can be easily proven that all the solenoidal and nonsolenoidal functions of the present MR basis are linear independent from each other. Therefore, the MR basis spans the same space as for the loop-star/tree basis.

B. The previous MR basis

The previous MR basis functions proposed in [18, 19] are constructed via SVD on charge matrices. After applying SVD on a charge matrix, the right singular vectors associated to non-zero and null singular values are assigned as the coefficients of the corresponding gRWG function to generate the solenoidal and nonsolenoidal MR functions respectively. However, the reason is not explained. In the following, a physical explanation to the above mathematical operations is given. Assuming a charge matrix generated by projecting *n* level-*l* gRWG functions onto *m* level-*l* cells, then its SVD result can be written as

$$\begin{aligned} [Q] &= \left[\nabla \cdot R_1, \nabla \cdot R_2, \cdots, \nabla \cdot R_n\right] = [U] \cdot [\Sigma] \cdot [V]^T \\ &= \left[U_1, U_2, \cdots, U_m\right] \cdot diag(\sigma_1, \sigma_2, \cdots, \sigma_{m-1}) \\ &\quad \left[V_1, V_2, \cdots, V_n\right]^T, \end{aligned} \tag{19}$$

where $\sigma_1 \geq \sigma_2 \geq \cdots \geq \sigma_{m-1} > 0$, since the rank of $[Q]$ is *m*-1. The expression (19) can be rewritten as

$$\begin{aligned} &\nabla \cdot \left[R_1, R_2, \cdots, R_n\right] \cdot \left[V_1, V_2, \cdots, V_n\right] = \\ &\left[\sigma_1 U_1, \sigma_2 U_2, \cdots, \sigma_{m-1} U_{m-1}, 0 \cdot U_m, \cdots, 0 \cdot U_n\right] \end{aligned}. \tag{20}$$

It can be inferred from (20) that the gRWG functions multiplies the first *m*-1 columns of $[V]$ generates *m*-1 linear independent functions which have surface charge and can be taken as the nonsolenoidal functions. Therefore, the number of the nonsolenoidal functions generated with the algorithm in [17, 18] can also be given by (18). Namely, the numbers of the MR nonsolenoidal functions in the present paper and in [17, 18] are equal. It can also be inferred from (20) that the gRWG functions multiplies the other *n*-*m* columns of $[V]$ generates *n*-*m* linear independent functions which have no surface charge and can be taken as the solenoidal functions.

It can be inferred from the discussion at the beginning of Section III that the number of the level-*l* solenoidal functions in a level-(*l*+1) cell (except the level-*L* cell of closed surfaces which

has no boundary) equals the number of the interior vertexes shared by the *level-l* edges inside the level-(l+1) cell. Furthermore, the number of the level-l solenoidal functions added by generating solenoidal functions across a pair of level-(l+1) cells equals the number of the interior vertexes which connecting the level-l edges that coincide with the common edge of the two level-(l+1) cells. Therefore, the total number of the MR basis functions generated in [18, 19] can be finally described by (21). It can be proven by theorem 1 that the number of the MR basis functions equals the number of the RWG basis functions of the input mesh.

Theorem 1 *The number of the RWG basis functions of the input mesh can be written as the sum of the following elements:*

$$N = \sum_{l=0}^{L} N_e^l + \sum_{l=1}^{L} \left(\sum_{n=1}^{N_e^l} N_{v,n}^l \right), \tag{21}$$

where N_e^l *(l=L) is the number of the level-L interior edges and* $N_e^l = \sum_{m=1}^{N_c^{l+1}} N_{e,m}^l$ *(0⩽l<L-1) is the total number of the level-l interior edges inside all level-(l+1) cells, in which* $N_{e,m}^l$ *is the number of the level-l edges inside the m-th level-(l+1) cell and* N_c^{l+1} *is the number of level-(l+1) cells, and* $N_{v,n}^l$ *is the number of the interior vertexes on the n-th level-l interior edges.*

Proof: The expression (21) can be interpreted by the changes of the interior edges of each level in the procedure of generating the hierarchical meshes. In the first step of the mesh generating procedure, the level-1 mesh is generated from the input mesh (level-0) and parts of the level-0 interior edges are grouped into the level-1 interior edges. Since the number of the level-0 interior edges grouped into one level-1 interior edge equals the number of the level-0 interior vertexes on the level-1 interior edge plus one, the total number of the grouped level-0 interior edges equals the total number of level-0 interior vertexes on the level-1 interior edges plus the number of the level-1 interior edges. Namely, the number of the level-0 interior edges can be decomposed as the sum of the total number of the level-0 interior edges inside all level-1 cells (i.e. the number of the left level-0 interior edges), the total number of level-0 interior vertexes on the level-1 interior edges, and the number of the level-1 interior edges. Similarly, the number of the level-l ($1 \leqslant l<L$-1) interior edges can be decomposed as the sum of the total number of the level-l interior edges inside all level-(l+1) cells, the total number of level-l interior vertexes on the level-(l+1) interior edges, and the number of the level-(l+1) interior edges. As a consequence, the number of the level-0 interior edges can be finally written as (21). Since each RWG basis function of the input mesh is corresponding to a level-0 interior edge, theorem 1 is proven.

It can be inferred from the above discussion that the number of the solenoidal and nonsolenoidal functions of the previous MR basis functions can also be given by equations (9)-(11). The level-L functions of the previous MR basis should be constructed independently if the cells are not finally grouped into one big cell. The level-L functions of the previous MR basis could be generated by applying SVD on the charge matrix generated by projecting the level-L gRWG functions on the level-L cells or simply taking the level-L gRWG basis functions as the level-L MR basis functions. It can also be inferred from Theorem 1 that the solenoidal part of the present MR basis can be constructed as a hierarchical basis in which each solenoidal function is generated as a linear combination of the gRWG functions of the same level which constitute a loop around an interior vertex.

V. COMPUTATIONAL COMPLEXITY

Since the computational complexity of the loop basis is known as $O(N)$ [28], only the computational complexity of the nonsolenoidal MR basis is needed to be analyzed. The computational complexity of the nonsolenoidal MR basis can be estimated by estimating the number of on-zero elements of the basis-changing matrix [T].

The number of non-zero elements of the basis-changing matrix [T] as the functions of the number of levels of a structure discretized with 19090 unknowns is investigated and shown in Fig. 3. It can be observed from Fig. 3 that the number of non-zero elements of matrix [T] increase linearly with the number of the levels of the MR basis. Therefore, the computational complexity of the

nonsolenoidal MR basis is of $O(NL)$, where L is the number of levels. If keep grouping the cells of each level upwards until the cells are finally grouped into one single cell in the highest level mesh, the number of levels L will be equal to Log$N$ and the computational complexity will be of $O(N\text{Log}N)$. The number of non-zero elements and the generation time of matrix [T] as functions of the number of the unknowns for the previous MR basis and present MR basis when the cells are finally grouped into a single cell are investigated and shown in Fig. 4 (a) and (b), respectively. It can be observed from the figure that the computational complexity of both the previous and present MR basis is of $O(N\text{Log}N)$ and the computational complexity of the present MR basis has a smaller constant.

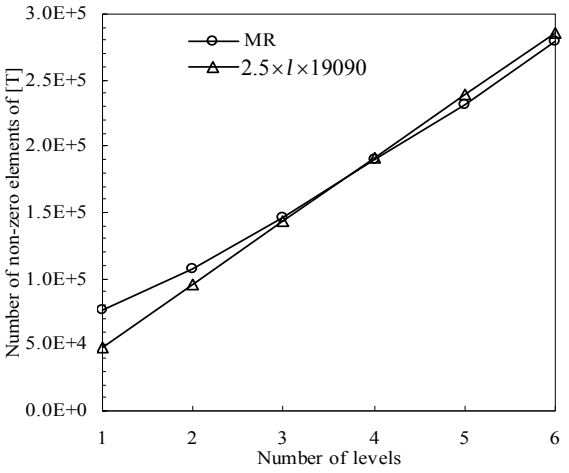

Fig. 3. The number of non-zero elements of the basis-changing matrix [T] versus the number of levels of a structure discretized with 19090 unknowns.

VI. NUMERICAL RESULTS

In this section, the MR basis is applied for the analysis of EM scattering problems at low frequencies. In the following examples, the restarted GMRES(30) algorithm is used as an iterative method. All simulations were performed on a PC computer with Intel(R) Core(TM)2 1.86 GHz CPU and 2 GB RAM using single precision. Zero vector is taken as initial approximate solution and the iteration process is terminated when the relative backward error is reduced by 10^{-4}. And all the results with different bases were obtained after applying a diagonal preconditioning to the MoM matrix.

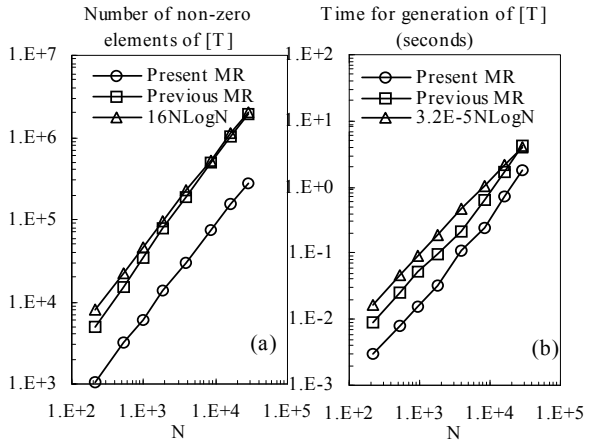

Fig. 4. (a) The number of non-zero elements of the basis-changing matrix [T], (b) the time for generation of matrix [T], versus the number of unknowns.

A. Offset bend rectangular cavity

The first example is a metallic offset bend rectangular cavity with 8.7 cm by 10 cm square cross section and offset angles 30°. As shown in Fig. 5, the offset bend rectangular cavity is discretized with 4317 unknowns. The mesh of the offset bend rectangular cavity could generate six levels hierarchical meshes and five levels MR basis at most. The EM scattering of the offset bend rectangular cavity is calculated with the EFIE using the RWG, loop-tree, the previous MR, and present MR bases. The 2-norm condition number and convergence behavior of GMRES(30) for the offset bend rectangular cavity using the above bases over a frequency range of 0.1-200 MHz is shown in Fig. 5 and Fig. 6, respectively. The corresponding total time for applying the MR bases is depicted in Fig. 7.

With reference to the figures, the RWG basis performs worse than both the loop-tree basis and MR bases in the low frequency range. It can be also found that the MR bases perform much better than the loop-tree basis in the low frequency range. The more levels of the present MR basis, the better it performs in the low frequency range. Comparing the previous MR basis with the present MR basis, it can be found that the present MR basis performs similar to the previous MR basis at low frequencies. However, the previous MR basis

performs more stable as the frequency increases. The corresponding total time which includes the time of the generation of the basis-changing matrix, the time of the generation of the diagonal preconditioning matrix, and the solution time of the GMRES(30) is depicted in Fig. 6. The result using the RWG basis is not given in Fig. 6 since the GMRES(30) solver cannot converge by using the RWG basis at some frequencies. It is also clearly indicates that the MR bases have better performance than the loop-tree basis at the low-frequency range.

The impact of the discretization density to the performance of different bases is investigated. The 2-norm condition number of the MoM matrices using the RWG basis, loop-tree basis, and the present and previous MR bases for the offset bend rectangular cavity discretized with different number of unknowns is shown in Fig. 8. It can be found from Fig. 8 that the MR bases perform more stable than the RWG basis and loop-tree basis as the discretization density increases and this result agrees with the results in [11].

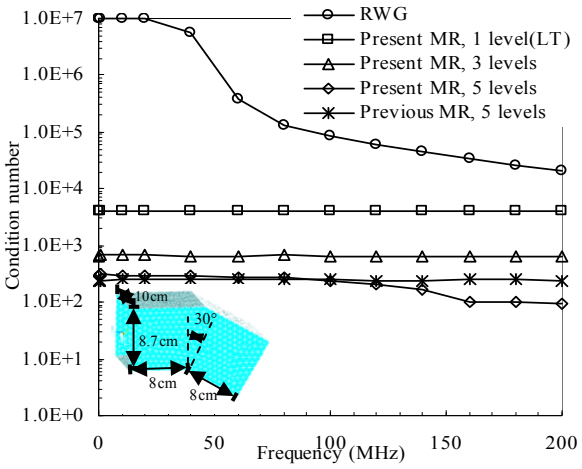

Fig. 5. The 2-norm condition number as a function of frequency for the offset bend rectangular cavity using the RWG, loop-tree, and MR bases.

B. Tank model

As shown in Fig. 9, the second example is a tank model discretized with 8706 unknowns. The length, width, and height of the tank model are 10.3 m, 3.3 m, and 2.3 m, respectively. To describe the shape of the tank model efficiently, the parts varying rapidly in geometry are discretized with relatively small triangular patches and the other parts are with large patches.

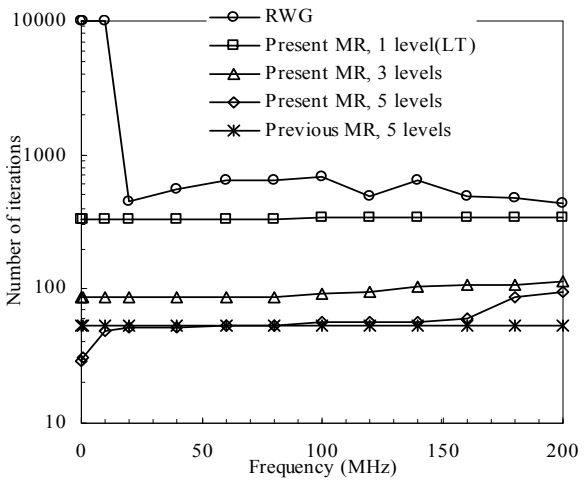

Fig. 6. The convergence behavior of GMRES(30) as a function of frequency for the offset bend rectangular cavity using the RWG, loop-tree, and MR bases.

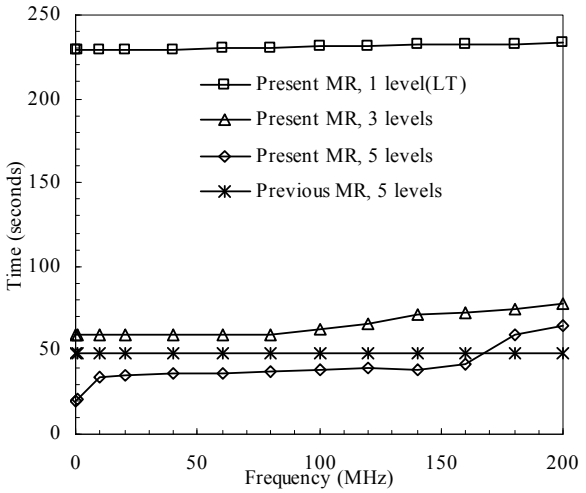

Fig. 7. The total time as a function of frequency for the offset bend rectangular cavity using the loop-tree and MR bases.

The convergence curves of the GMRES(30) are compared in Fig. 9 at the low frequency 1.0 MHz using the RWG, loop-tree and the MR bases. It can also be found from Fig. 9 that the convergence of the GMRES(30) using the MR bases which have higher levels is much faster than the others. The convergence behavior of GMRES(30) and the corresponding total time for applying the MR bases over a frequency range of

0.1-6 MHz is shown in Fig. 10 and Fig. 11, respectively. From Fig. 10 and Fig. 11 it can found that the both MR basis performs similar at lower frequencies and the previous MR performs more stable as the frequency increases.

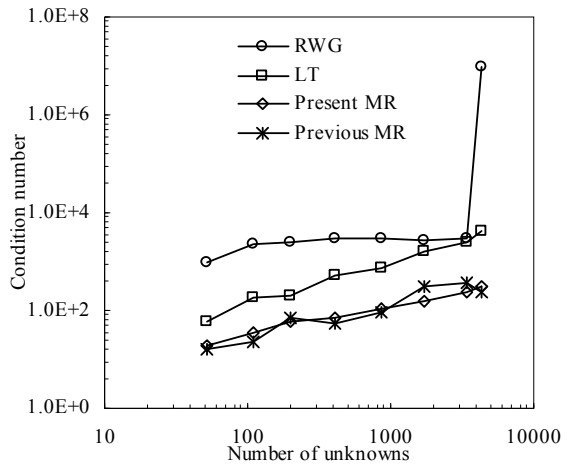

Fig. 8. The 2-norm condition number as a function of discretization density for the offset bend rectangular cavity using the RWG, loop-tree, and MR bases.

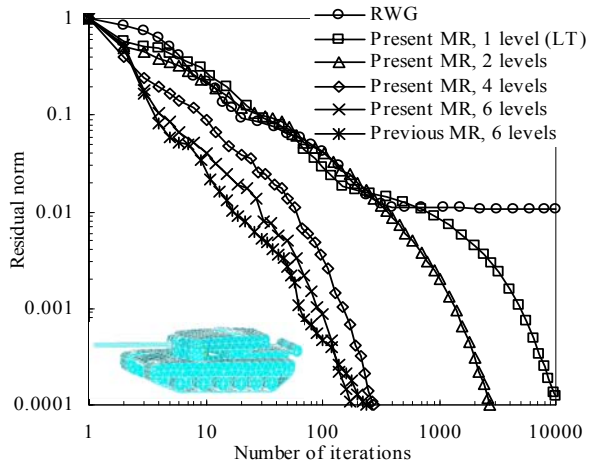

Fig. 9. The convergence history of the GMRES(30) for the tank model at 1.0 MHz using the RWG, loop-tree, and MR bases.

VII. CONCLUSION

An alternative MR basis has been proposed for analyzing low-frequency problems using the MoM. Contrary to the previous MR basis which is generated based on mathematical operations, the present MR basis is generated based on geometrical operations. The present MR basis is an extension of the loop-tree basis to hierarchical basis, and the loop-tree can be treated as a special one-level MR basis.

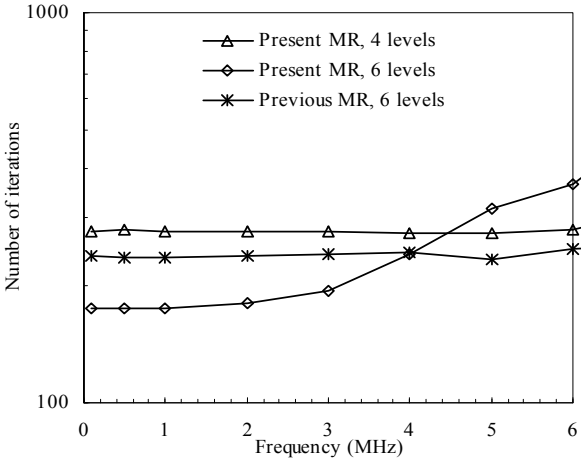

Fig. 10. The convergence behavior of GMRES(30) as a function of frequency for the tank model using the MR bases.

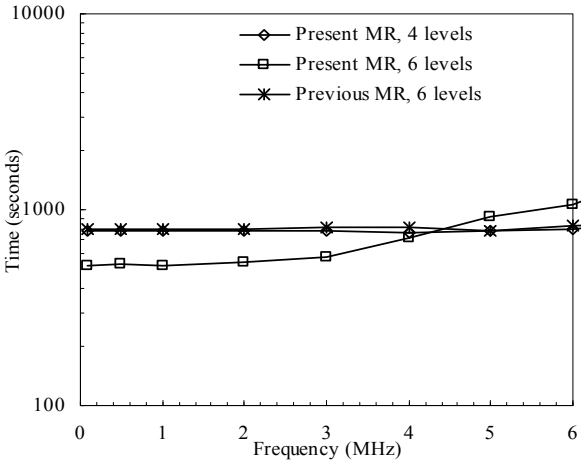

Fig. 11. The total time as a function of frequency for the tank model using the MR bases.

Therefore, the present MR basis is easier to construct and comprehend. Also, the computational complexity of the present MR basis is lower than that of the previous MR basis and the basis-changing matrix of the RWG basis to the present MR basis is sparser. As similar to the loop-tree basis, the present MR basis functions are combinations of RWG basis functions. Thus, the present MR basis can be easily applied to existing MoM codes. It has been demonstrated by the numerical results that the MR bases can be used to solve low-frequency EM scattering problems

efficiently. Compared with the traditional loop-tree basis, the MR bases converge much faster at low frequencies for iterative solvers. Although the present MR basis performs similar to the previous MR basis at lower frequencies, it should be pointed out that the present MR basis suffers the same drawback as the loop-tree basis, i.e. it will be unstable as the frequency goes higher. Therefore, the previous MR basis is recommended at higher frequencies since it performs more stable as the frequency increases.

ACKNOWLEDGMENT

The authors would like to thank the assistance and support of Major State Basic Research Development Program of China (973 Program: 2009CB320201), Natural Science Foundation of 60871013, 60701004, and 60928002, and Jiangsu Natural Science Foundation of BK2008048.

REFERENCES

[1] R. F. Harrington, *Field Computations by Moment Methods*, MacMillan, New York, 1968.

[2] S. M. Rao, D. R. Wilton, and A. W. Glisson, ‘‘Electromagnetic Scattering by Surfaces of Arbitrary Shape,’’ *IEEE Trans. Antennas Propagat.*, vol. AP-30, pp. 409-418, May 1982.

[3] D. R. Wilton and A.W. Glisson, “On Improving the Electric Field Integral Equation at Low Frequencies,” in *Proc. URSI Radio Science Meeting Dig.*, Los Angeles, CA, p. 24, June 1981.

[4] J. Mautz and R. F. Harrington, “An E-Field Solution for a Conducting Surface Small or Comparable to the Wavelength,” *IEEE Trans. Antennas Propagat.*, vol. AP-32, no. 4, pp. 330-339, April 1984.

[5] M. Burton and S. Kashyap, “A Study of a Recent Moment-Method Algorithm that is Accurate to Very Low Frequencies,” *Applied Computational Electromagnetic Society (ACES) Journal*, vol. 10, no. 3, pp. 58-68, Nov. 1995.

[6] W. L. Wu, A. Glisson, and D. Kajfez, “A Study of Two Numerical Solution Procedures for the Electric Field Integral Equation at Low Frequency,” *Applied Computational Electromagnetic Society (ACES) Journal*, vol. 10, no. 3, pp. 69-80, Nov. 1995.

[7] G. Vecchi, “Loop-Star Decomposition of Basis Functions in the Discretization of the EFIE,” *IEEE Trans. Antennas Propagat.*, vol. 47, no. 2, pp. 339-346, Feb. 1999.

[8] J. S. Zhao and W. C. Chew, “Integral Equation Solution of Maxwell’s Equations from Zero Frequency to Microwave Frequency,” *IEEE Trans. Antennas Propagat.*, vol. 48, pp. 1635-1645, Oct. 2000.

[9] J. F. Lee, R. Lee, and R. J. Burkholder, “Loop Star Basis Functions and a Robust Precodnitioner for EFIE Scattering Problems,” *IEEE Trans. Antennas Propagat.*, vol. 51, pp. 1855-1863, Aug. 2003.

[10] T. F. Eibert, “Iterative-Solver Convergence for Loop-Star and Loop-Tree Decomposition in Method-of-Moments Solutions of the Electric-Field Integral Equation,” *IEEE Antennas Propag. Mag.*, vol. 46, pp. 80-85, Jun. 2004.

[11] F. P. Andriulli, A. Tabacco, and G. Vecchi, “Solving the EFIE at Low Frequencies with a Conditioning that Grows Only Logarithmically with the Number of Unknowns,” *IEEE Trans. Antennas Propagat.*, vol. 58, no. 5, pp. 1614-1624, May 2010.

[12] F. Vipiana, P. Pirinoli, and G. Vecchi, “A Multiresolution Method of Moments for Triangular Meshes,” *IEEE Trans. Antennas Propag.*, vol. 53, no. 7, pp. 2247-2258, Jul. 2005.

[13] F. Vipiana, G. Vecchi, and P. Pirinoli. “A Multiresolution System of Rao–Wilton–Glisson Functions,” *IEEE Trans. Antennas Propagat.*, vol. 55, no. 3, pp. 924-930, Mar. 2007.

[14] F. Andriulli, A. Tabacco, and G. Vecchi, “A Multiresolution Approach to the Electric Field Integral Equation in Antenna Problems,” *SIAM J. Sci. Comput.*, vol. 29, pp. 1-21, Jan. 2007.

[15] R. S. Chen, J. J. Ding, D. Z. Ding, Z. H. Fan, and D. X. Wang, “A Multiresolution Curvilinear Rao-Wilton-Glisson Basis Function for Fast Analysis of Electromagnetic Scattering,” *IEEE Trans. Antennas Propagat.*, vol. 57, no. 10, pp. 3179-3188, Oct., 2009.

[16] F. P. Andriulli, F. Vipiana, and G. Vecchi, “Enhanced Multiresolution Basis for the MoM Analysis of 3D Structures,” in *Proc. IEEE Int. Symp. Antennas Propagat.*, Honolulu, HI, Jun. 2007, pp. 5612-5615.

[17] F. P. Andriulli, F. Vipiana, and G. Vecchi, "Hierarchical Bases for Non-Hierarchic 3-D Triangular Meshes," *IEEE Trans. Antennas Propagat.*, vol. 56, pp. 2288-2297, Aug. 2008.

[18] F. Vipiana, F. P. Andriulli, and G. Vecchi, "Two-Tier Non-Simplex Grid Hierarchic Basis for General 3D Meshes," *Waves in Random and Complex Media*, vol. 19, no. 1, Feb. 2009, pp.126-146.

[19] F. Vipiana, and G. Vecchi, "A Novel, Symmetrical Solenoidal Basis for the MoM Analysis of Closed Surfaces," *IEEE Trans. Antennas Propagat.*, vol. 57, no. 4, pp. 1294-1299, April 2009.

[20] F. Vipiana, P. Pirinoli, and G. Vecchi, "Regularization Effect of a Mutiresolution Basis on the EFIE-MoM Matrix," *IEEE Antennas and Propagation Society Int. Symp. Digest*, Washington, DC, Jul. 2005, vol. 3b, pp. 192-195.

[21] F. Vipiana, P. Pirinoli, and G. Vecchi, "Spectral Properties of the EFIE-MoM Matrix for Dense Meshes with Different Types of Bases," *IEEE Trans. Antennas Propagat.*, vol. 55, no. 11, pp. 3229-3238, Nov. 2007.

[22] J. J. Ding, J. Zhu, D. Z. Ding, and R. S. Chen, "Application of Perturbed Multiresolution Preconditioner Technique Combined with MLFMA for Scattering Problem," in *Proc. Int. Conf. on Microwave and Millimeter Wave Technology*, pp. 978-981, Apr. 2008.

[23] H. Chen, D. Z. Ding, R. S. Chen, D. X. Wang, and E. K. Yung, "Application of Multiresolution Preconditioner Technique for Scattering Problem in a Half Space," in *Proc. Int. Conf. on Microwave and Millimeter Wave Technology*, pp. 975-977, Apr. 2008.

[24] Y. Q. Hu, J. J. Ding, D. Z. Ding, and R. S. Chen, "Analysis of Electromagnetic Scattering from Dielectric Objects above a Lossy Half-Space by Multiresolution Preconditioned Multilevel Fast Multipole Algorithm," *IET Microw. Antennas Propag.*, vol. 4, iss. 2, pp. 232-239, Feb., 2010.

[25] M. M. Li, J. J. Ding, D. Z. Ding, Z. H. Fan, and R. S. Chen, "Multiresolution Preconditioned Multilevel UV Method for Analysis of Planar Layered Finite Frequency Selective Surface," *Microwave and Optical Technology Letters*, vol. 52, no. 7, pp. 1530-1536, July 2010.

[26] F. Vipiana, M. A. Francavilla, and G. Vecchi, "A Multi-Resolution Stabilization of the Incomplete LU Preconditioner," in *Antennas and Propagation Society International Symposium*, Charleston, SC, June 2009, pp. 1-4.

[27] F. Vipiana, M. A. Francavilla, and G. Vecchi, "EFIE Modeling of High-Definition Multiscale Structures," *IEEE Trans. Antennas Propagat.*, vol. 58, no. 7, pp. 2362-2374, July 2010.

[28] F. Vipiana, G. Vecchi, and D. R. Wilton, "Automatic Loop-Tree Scheme for Arbitrary Conducting Wire-Surface Structures," *IEEE Trans. Antennas Propagat.*, vol. 57, no. 11, pp. 3564-3574, Nov. 2009.